Electronic Supporting Information (ESI)

Synergistic photothermal and photocatalytic membrane for efficient solar-driven contaminated water treatment

Yang Ding[a], Kai Feng[a], Panpan He[a], Ning Liu[a], Liang Hao[a], Jiang Gong*[,a], Ran Niu*[,a], Jinping Qu*[,a,b]

[a] Key Laboratory of Material Chemistry for Energy Conversion and Storage, Ministry of Education, Hubei Key Laboratory of Material Chemistry and Service Failure, Hubei Engineering Research Center for Biomaterials and Medical Protective Materials, School of Chemistry and Chemical Engineering, Huazhong University of Science and Technology, Wuhan 430074, China.

[b] National Engineering Research Center of Novel Equipment for Polymer Processing, Key Laboratory of Polymer Processing Engineering, Ministry of Education, Guangdong Provincial Key Laboratory of Technique and Equipment for Macromolecular Advanced Manufacturing, School of Mechanical and Automotive Engineering, South China University of Technology, Guangzhou 510641, China.

E-mail addresses: gongjiang@hust.edu.cn (J. Gong); niuran@hust.edu.cn (R. Niu); jpqu@hust.edu.cn (J.P. Qu)

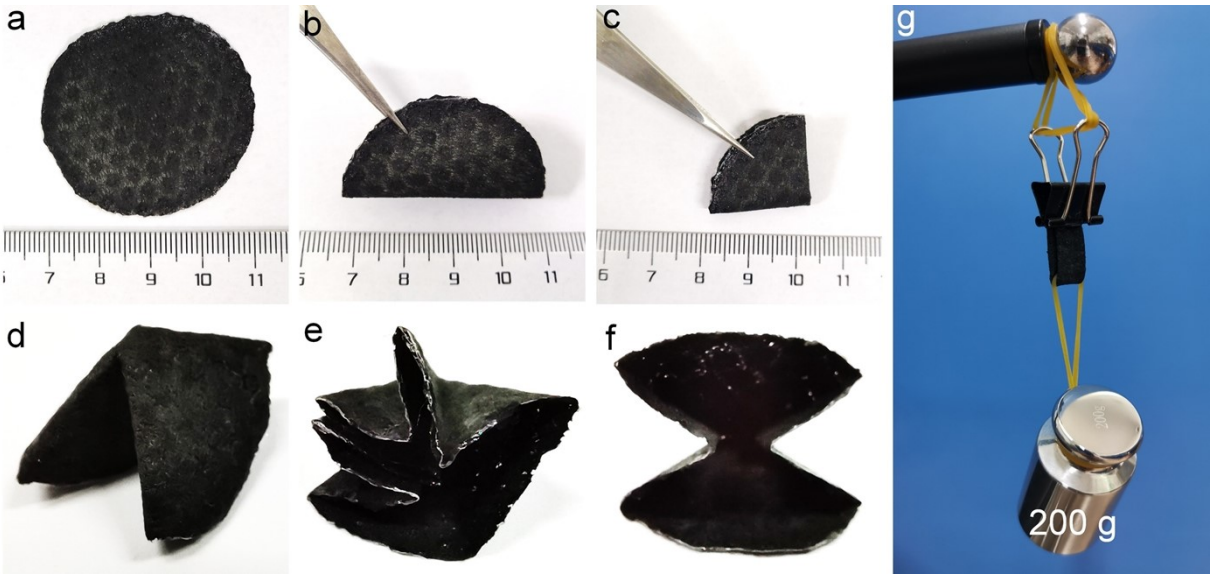

Fig. S1 Optical images showing (a-f) the flexibility and (g) robust mechanical property of CNMC-5 membrane.

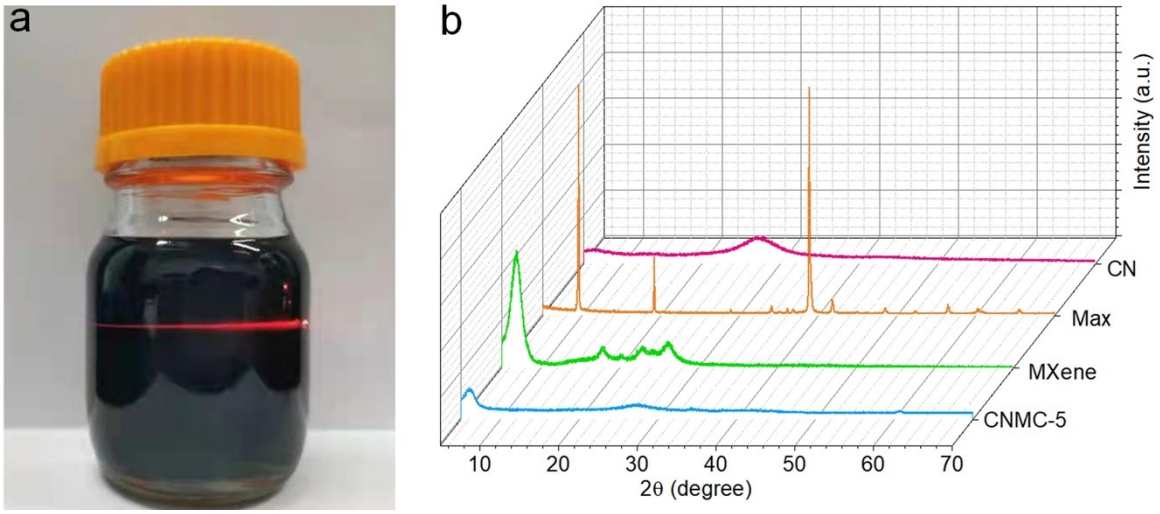

Fig. S2 (a) Photograph of MXene suspension. (b) XRD profiles of CN, MAX, MXene, and CNMC-5.

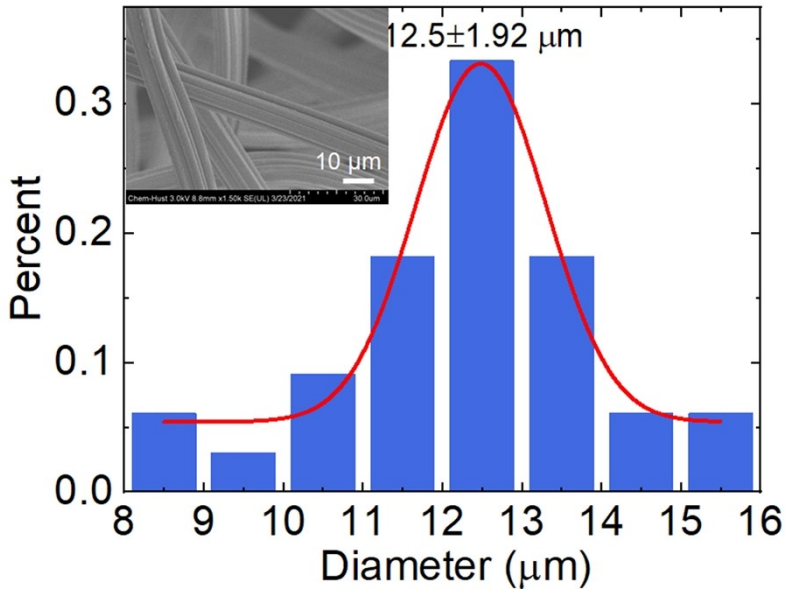

Fig. S3 The diameter distribution plot of cotton cloth fiber. The inset shows the SEM image of cotton cloth fiber.

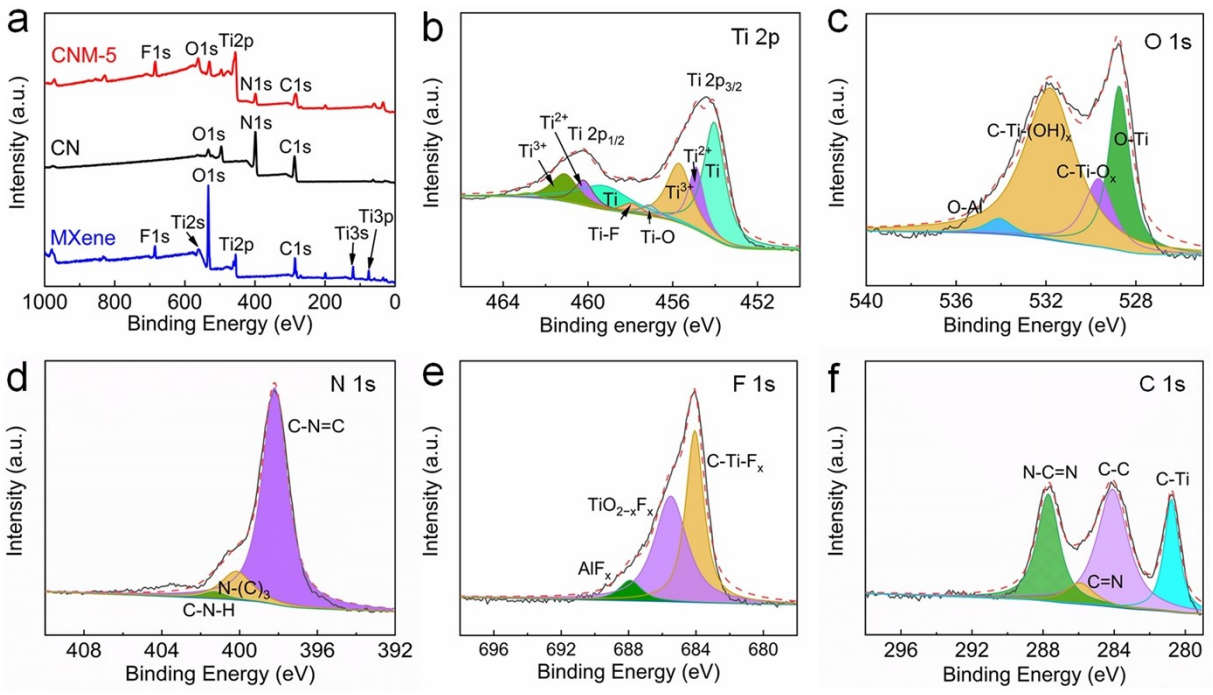

Fig. S4 (a) The full scan XPS spectra of MXene, CN and CNM-5. High-resolution (b) Ti 2p, (c) O 1s, (d) N 1s, (e) F 1s, and (f) C1s spectra of CNM-5 hybrid material.

Note: The surface element composition and chemical states of sample were examined by XPS. The survey spectrum of CNM-5 demonstrates the existence of F, Ti, C, O and N (Fig. S4a), and their atomic contents are listed in Table S1. As displayed in Fig. S4b, high-resolution Ti 2p XPS spectrum is deconvoluted to components corresponding to Ti bound to C, Ti^{2+}, Ti^{3+} and

Ti bound to O and F, typical of $Ti_3C_2T_x$ [1,2]. The peaks at 461.5 and 455.8 eV are assigned to the Ti^{3+} $2p_{3/2}$ and $2p_{1/2}$, respectively, while the peaks at 460.2 and 455.0 eV are allocated to the Ti^{2+} $2p_{3/2}$ and $2p_{1/2}$, respectively [1,2]. The peaks in the high-resolution O 1s spectrum indicates the presence of O-Ti, C-Ti-O_x, C-Ti-$(OH)_x$, and O-Al bonds, respectively, based on the peaks at 528.7, 529.7, 531.8 and 534.1 eV (Fig. S4c). The high-resolution C 1s XPS spectrum presents the existence of N-C=N, C=N, C-C and C-Ti bonds assigned to the peaks at 287.7, 285.9, 284.1 and 280.8 eV, respectively (Fig. S4f) [2,3].

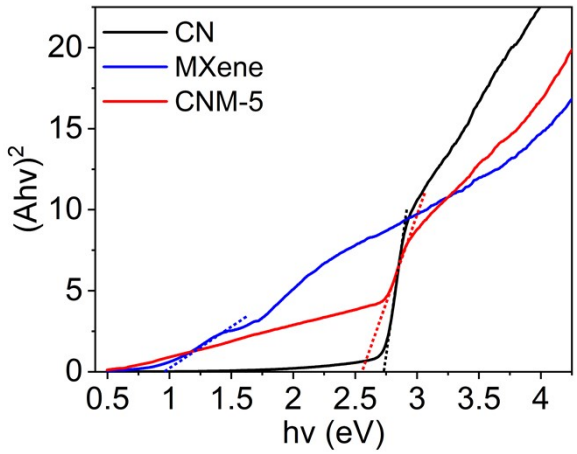

Fig. S5 Kubelka-Munk plots and energy gap estimation of CN, MXene and CNM-5.

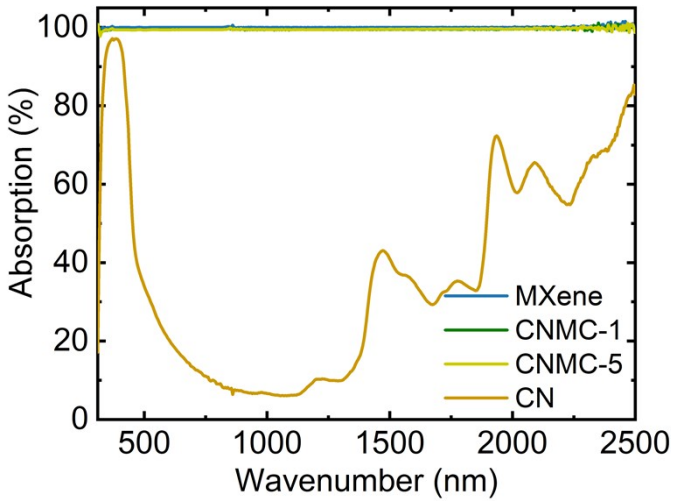

Fig. S6 UV-Vis-NIR absorption spectra of pristine cloth, CNMC-1, CNMC-5 and CN.

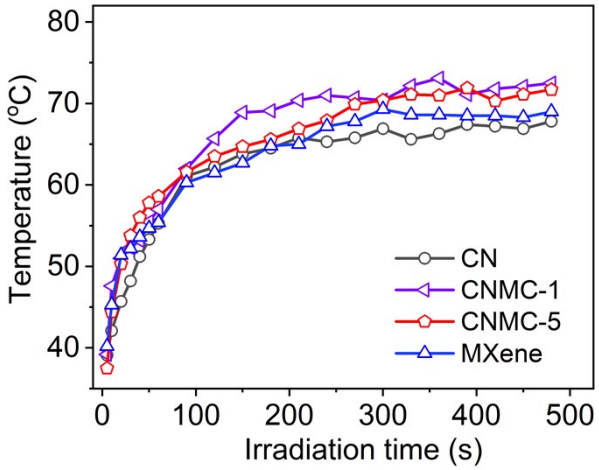

Fig. S7 Surface temperature curves of CNMC-1, CNMC-5, MXene and CN-coated cloth under 1 kW m^{-2} visible light irradiation.

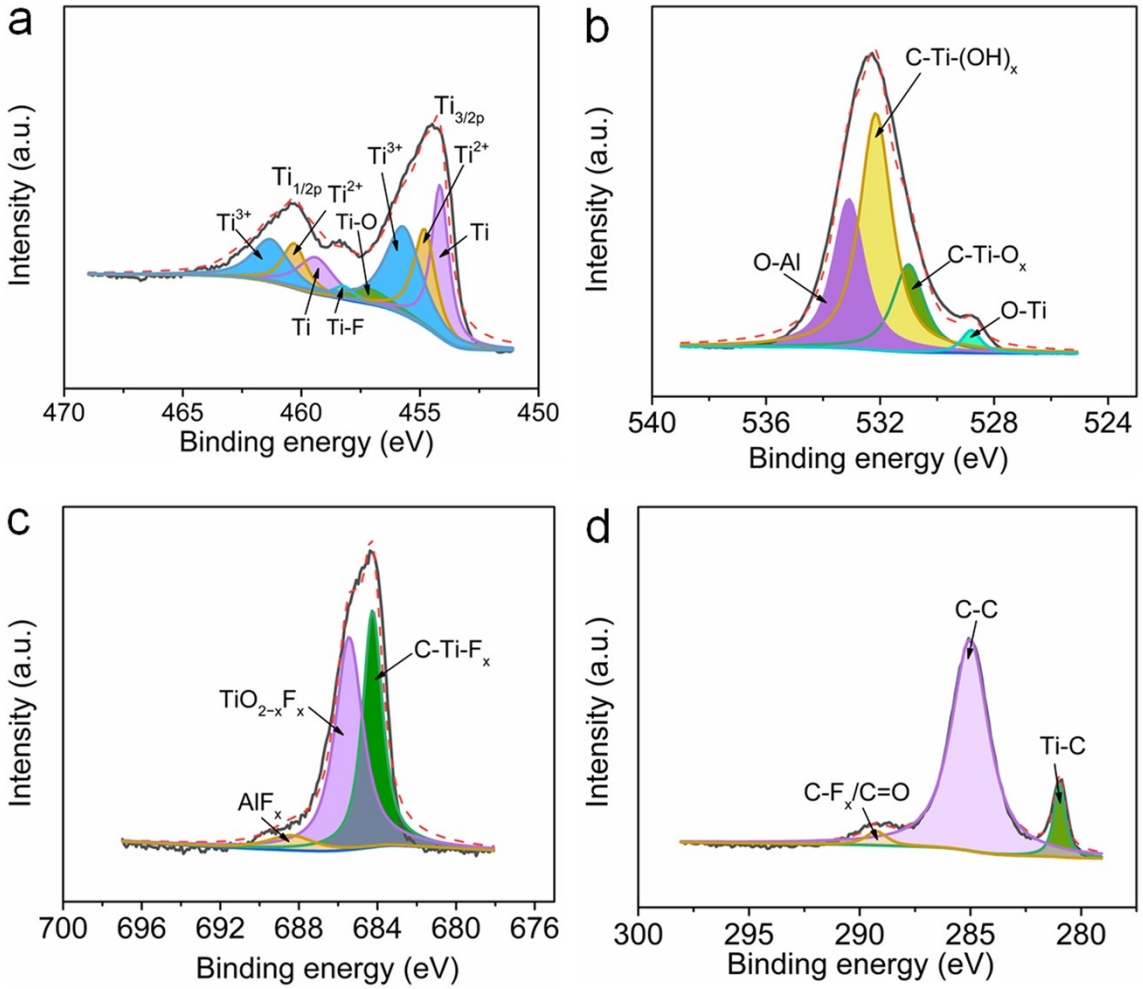

Fig. S8 High-resolution (a) Ti 2p, (b) O 1s, (c) F 1s, and (d) C1s spectra of MXene.

Note: The surface fluorine- and oxygen-containing functional groups could to an extent improve the hydrophilicity of MXene.

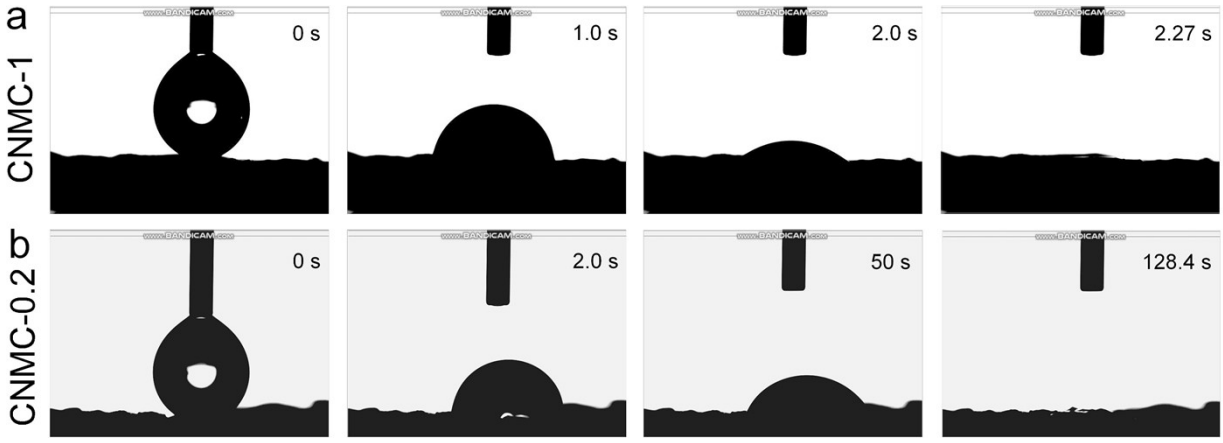

Fig. S9 Time evolution of the water contact angles of (a) CNMC-1 and (b) CNMC-0.2.

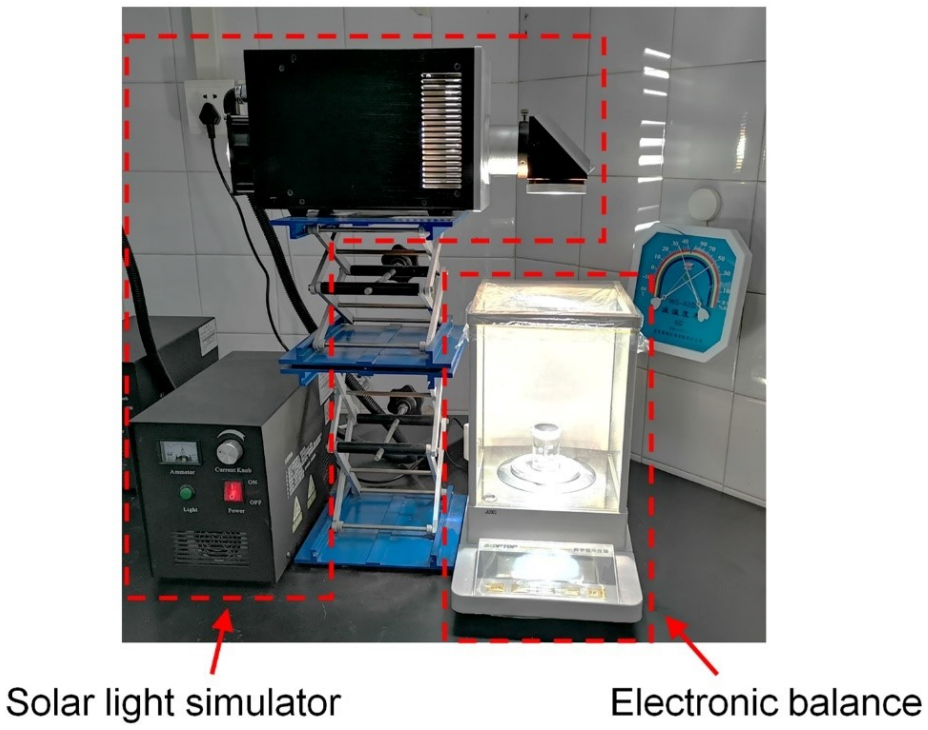

Fig. S10 Photograph of interfacial solar vapor generation system used in this work.

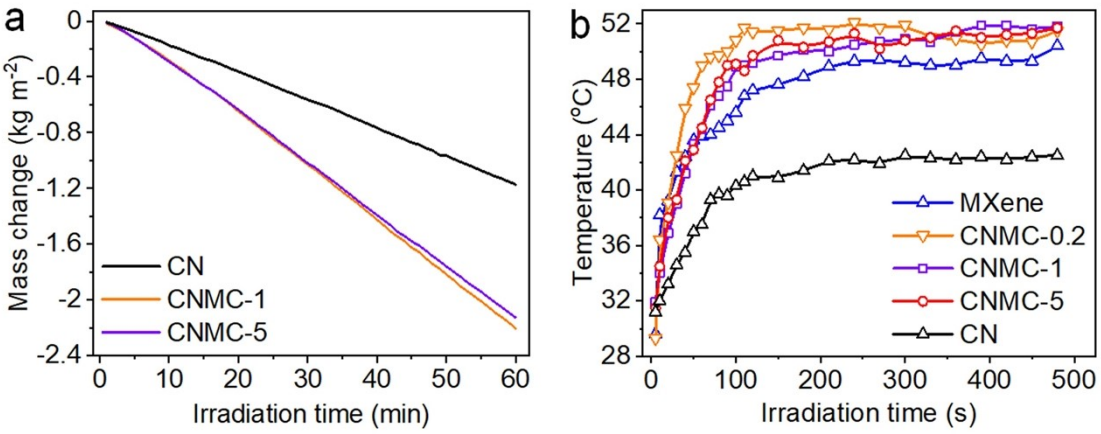

Fig. S11 (a) Water mass changes as a function of irradiation time of CNMC-1, CNMC-5 and CN-coated cloth under 1 kW m^{-2} irradiation. (b) Surface temperature versus time of CNMC-0.2, CNMC-1, CNMC-5, MXene- and CN-coated cloth under 1 kW m^{-2} irradiation.

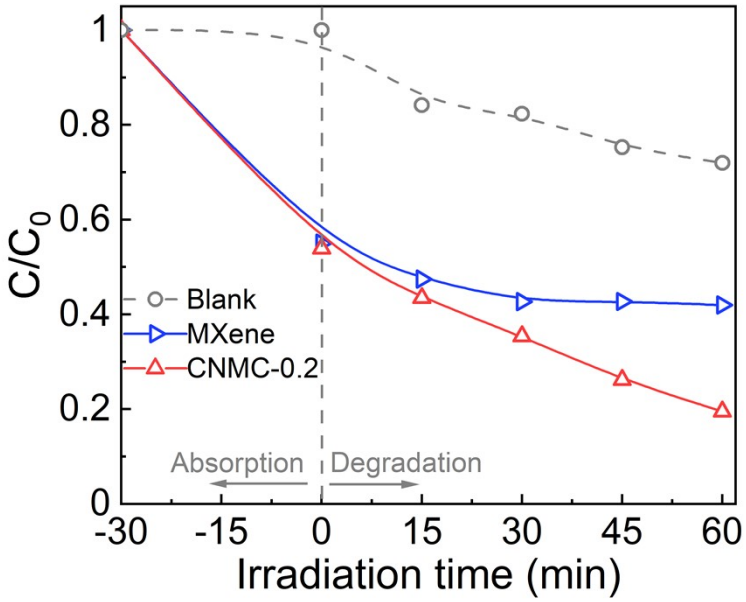

Fig. S12 Degradation of RhB by MXene and CNMC-0.2 under 1 kW m^{-2} irradiation.

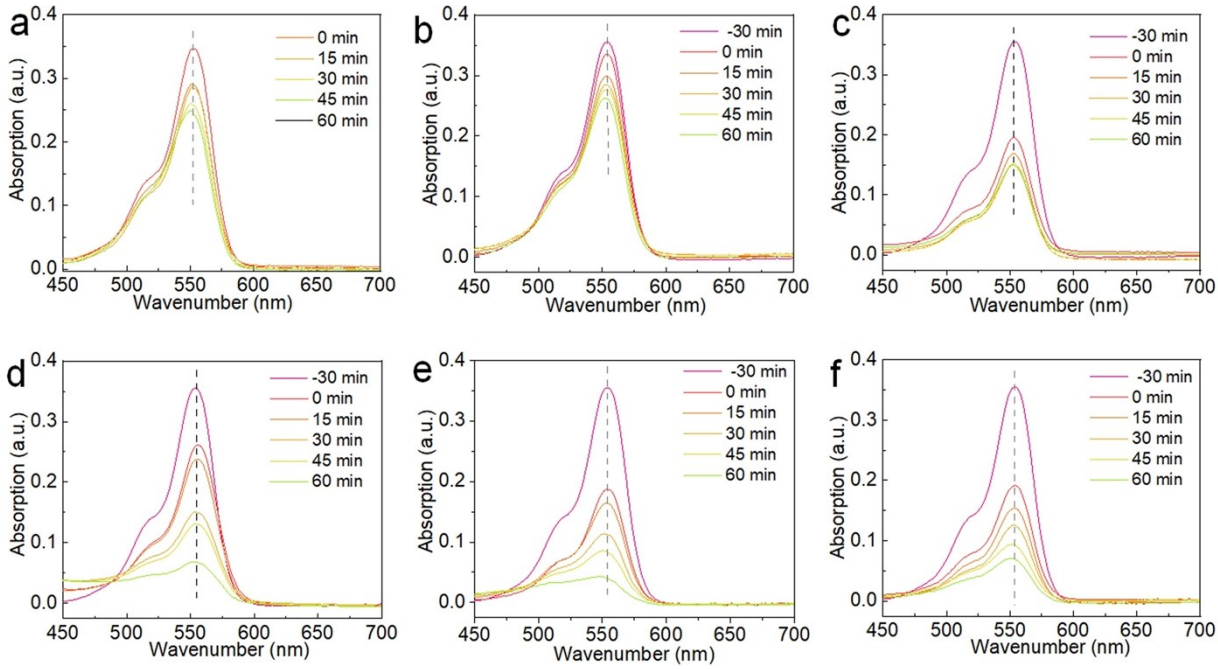

Fig. S13 UV-Vis absorption spectra of RhB at different time under different conditions: (a) without samples (i.e., blank), (b) cotton cloth, (c) MXene, (d) CN, (e) CNMC-1, and (f) CNMC-0.2.

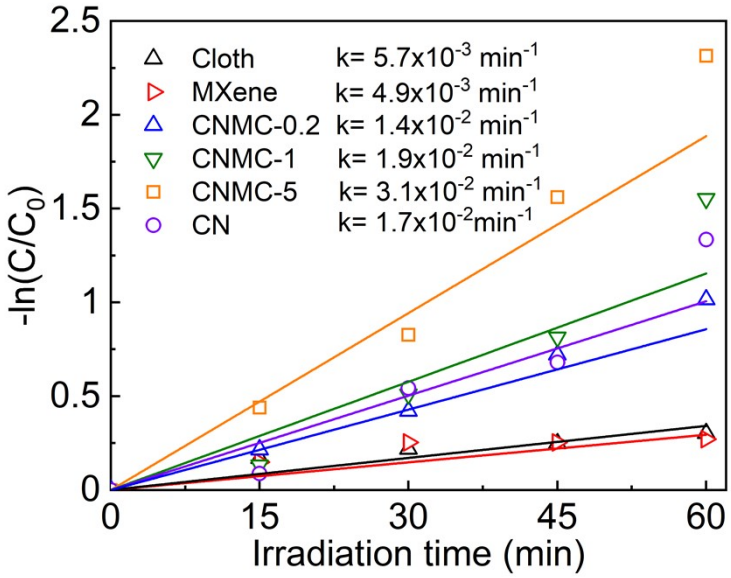

Fig. S14 Kinetic linear fitting curves of the photocatalytic degradation of RhB by different solar evaporators.

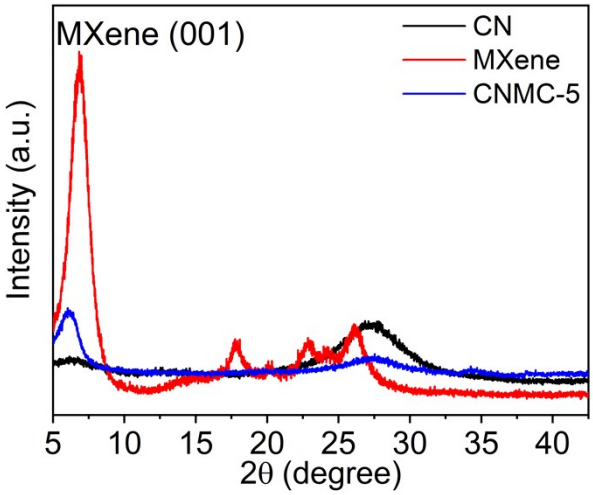

Fig. S15 XRD patterns of CN, MXene and CNMC-5.

Note: The (001) diffraction peak intensity of MXene is reduced greatly, suggesting the interaction of MXene and CN to an extent retards the stacking of MXene nanosheets.

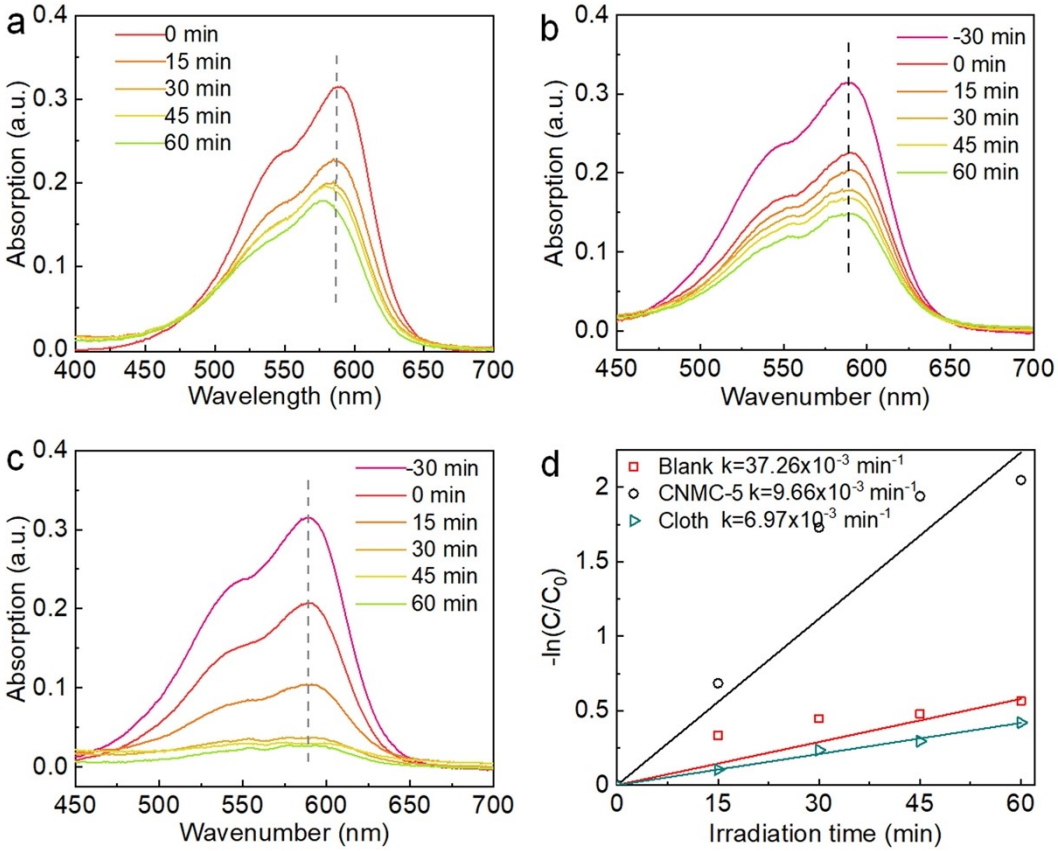

Fig. S16 UV-Vis absorption spectra of CV degraded photocatalysts (a) or by using cloth (b) and CNMC-5 (c) under 1 kW m^{-2} irradiation, and (d) their kinetic linear fitting curves.

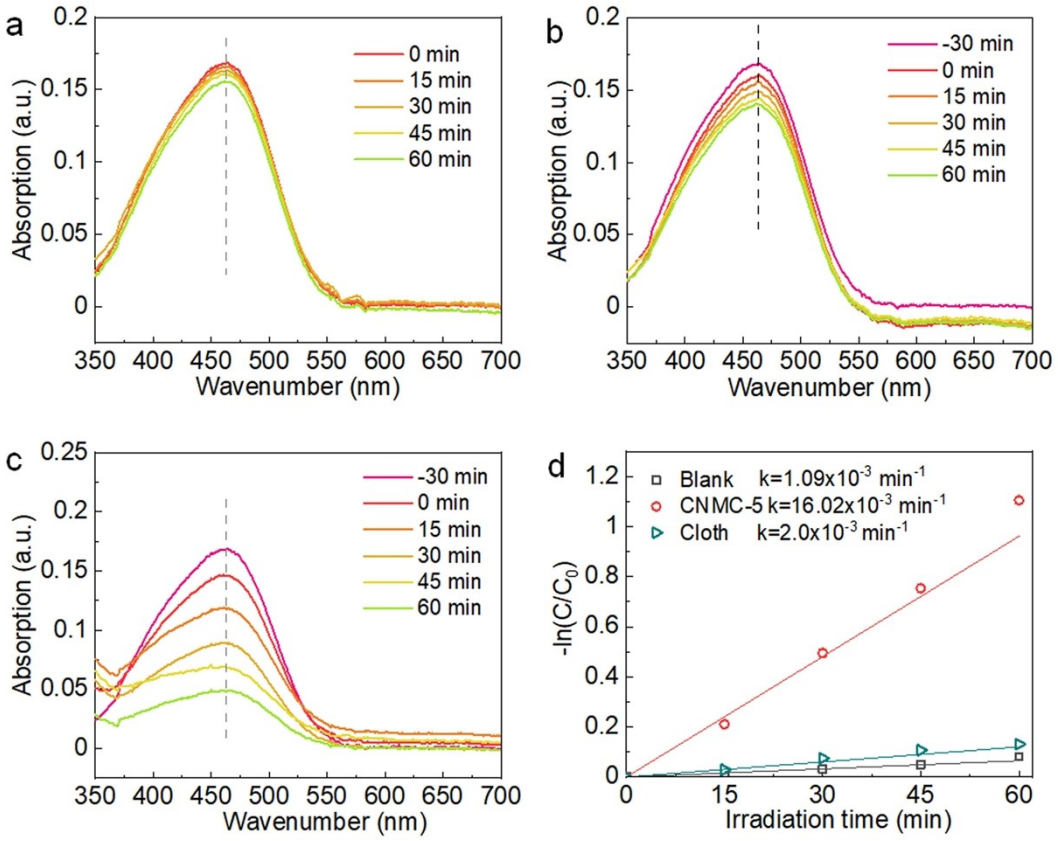

Fig. S17 UV-Vis absorption spectra of MO under different conditions: (a) blank (i.e., without photocatalysts), (b) cotton cloth, and (c) CNMC-5 under 1 kW m^{-2} irradiation. (d) The kinetic linear fitting curves of MO under different conditions.

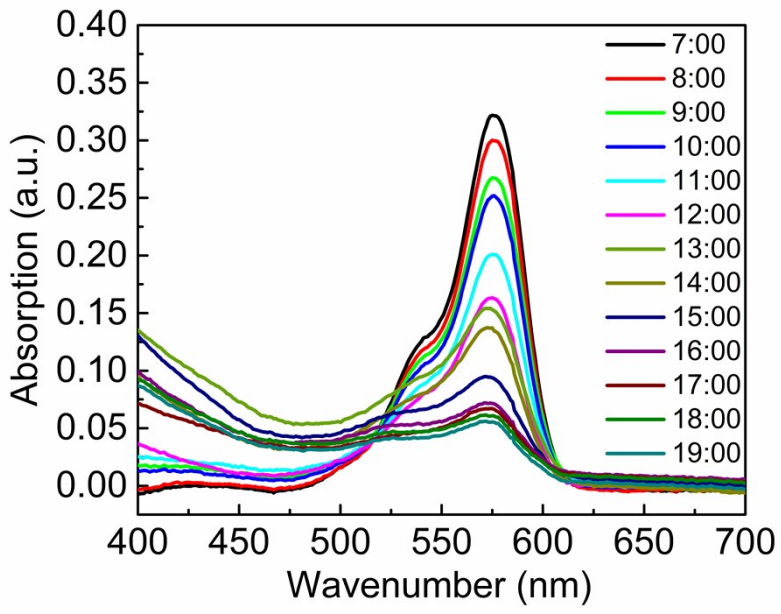

Fig. S18 UV-Vis absorption spectra of RhB solutions during the outdoor solar evaporation and photocatalytic experiments.

Table S1 XPS atomic contents of CN, MXene and CNM-5.

Atom	CNM-5	CN	MXene
C	39.87	45.03	33.75
F	9.81	0	7
N	16.2	47.29	0
O	19.5	7.67	52.63
Ti	14.62	0	6.62

Table S2 Thermal conductivity of different solar evaporators.

Sample	Thermal conductivity ($W\ m^{-1}\ K^{-1}$)
Cloth	0.058
MXene	0.098
CN	0.065
CNMC-0.2	0.080
CNMC-1	0.075
CNMC-5	0.074

Table S3 Comparison of solar steam generation performance of CNMC-0.2 with some previous photothermal materials under 1 kW m^{-2} irradiation.

Entry	Photothermal material	Evaporation rate ($kg\ m^{-2}\ h^{-1}$)	Efficiency (%)	Reference in SI
1	CNMC-0.2	2.33	98.9	This work
2	Co-CNS/M foam	1.39	93.1	4
3	CMF@d-Ti_3C_2	1.60	84.6	5
4	Co_3O_4/Ti_3C_2 MXene based fabric	1.89	130.4	6
5	GO/MXene aerogel	1.27	90.7	7
6	MXene on wood	1.46	96	8
7	MXene/PVA hydrogel	2.71	90.7	9

8	Janus MXene aerogel	1.46	87	10
9	SUC-700@W	2.07	91.5	11
10	Aluminophosphate-treated wood	1.42	90.8	12
11	Carbonized wood-slice	1.45	91.3	13
12	TiN/wood-derived carbon foam	1.47	92.5	14
13	Flexible wood membrane/CNTs	0.95	65	15
14	Carbonized longitudinal wood	1.08	74	16
15	ALD/Chinese ink coated wood	1.31	82.2	17
16	rGO-wood based aerogel	1.35	90.9	18
17	Ag@PDA wooden flower	2.08	97	19
18	Carbonized moldy bread	0.96	71.4	20
19	Carbonized E. prolifera	1.3	84	21
20	Carbonized mushrooms	1.48	78	22
21	N-doped porous graphene	1.50	80	23
22	Snake-scale-like porous carbon	1.58	91	24
23	rGO/cellous esters membrane	0.84	60	25
24	RGO-SA-CNT aerogel	1.62	83	26
25	3D graphene networks	1.64	91.8	27
26	Laser TiO_2/nickel foam	1.25	78.5	28

27	Au/disordered nanoporous template	0.80	64	29
28	Polypyrrole/stainless steel	0.92	58	30
29	Attapulgite/ poly acrylamide composite	1.2	85	31
30	PAN and PAN/GO bilayer membrane	2.27	92.6	32

Table S4 The calculation of the cost of CNMC-5.

Material	Cost	Remarks
MXene	¥ 33.01 g^{-1}	In this process, 2.5 g MAX, 87 mL HCl, 2.5 g LiF and 300 mL water are needed. The cost for the electricity and equipment is estimated as ¥ 0.5.
PVA	¥ 0.20 g^{-1}	It is obtained from Kuraray Co., Ltd (Japan).
CN	¥ 2.86 g^{-1}	In this process, 1.8 g melamine, 81 g NaCl, and 600 mL water are needed. The cost for the electricity and equipment is estimated as ¥ 1.0.
Cotton cloth	¥ 0.21 per piece	It is provided by GRACELAND Textile Co. Ltd (China).
CNMC-5 (in door)	¥ 0.25 per piece	In this process, 30 mg PVA, 25 mg CN, 5 mg MXene, 0.02 piece of cloth and 30 mL water are needed.
CNMC-5 (outdoor)	¥ 6.27 per piece	In this process, 750 mg PVA, 625 mg CN, 125 mg MXene, 1 piece of cloth and 500 mL water are needed.

Note S1 The analysis of heat loss

Generally, the heat loss of water evaporation process has three parts, including radiation, convection and conduction. The calculation detail of heat loss is shown as follows:

(1) Radiation

The radiation heat flux was calculated by the Stefan-Boltzmann equation:

$$\emptyset = \varepsilon A\sigma(T_1^4 - T_2^4) \quad \text{(S1)}$$

where $\emptyset$ represents heat flux, ε is the emissivity, and emissivity in the water evaporation processes is supposed to have a maximum emissivity of 1. A is the effective evaporation surface area. σ is the Stefan-Boltzmann constant (the value is 5.67×10^{-8} W m^{-2} K^{-4}). T_1 is surface temperature of the as-prepared materials after stable steam generation under one-sun illumination (ca. 51.5 ^{o}C, 324.65 K), and T_2 is the ambient temperature upward the absorber (ca. 47 ^{o}C, 320.15 K).

Then, the radiation loss can be calculated by:

$$\eta_{rad} = \Phi/P_{in} \quad \text{(S2)}$$

Under 1 kW m^{-2}, the radiation heat loss η_{rad} is calculated to be 2.2%.

(2) Convection

The convective heat loss is defined by Newton' law of cooling:

$$Q = hA\Delta T \quad \text{(S3)}$$

where Q is the the convection heat flux, h represents the convection heat transfer coefficient, which is approximately 5 W m^{-2} K^{-1}. ΔT is different between the surface temperature of CNMC-0.2 and the ambient temperature upward the absorber. Consequently, the convection heat loss of CNMC-0.2 was calculated through Equation S3, and the value is 1.5%.

(3) Conduction

$$Q = Cm\Delta T \quad \text{(S4)}$$

where Q is the heat energy, C represents the specific heat capacity of water (4.2 kJ K^{-1} kg^{-1}), and m denotes the weight of water (g). ΔT is the increased temperature of water. In this work, m = 15 g, ΔT = 0.5 K. Consequently, according to Equation S4, the calculated conduction heat loss of CNMC-0.2 is ca. 1.2%.

Therefore, the heat loss of CNMC-0.2 in the water evaporation is 4.9%.

Reference in supporting information

1. O. Mashtalir, K. M. Cook, V. N. Mochalin, M. Crowe, M. W. Barsoum and Y. Gogotsi, *J. Mater. Chem. A*, 2014, **2**, 14334-14338.
2. M. Alhabeb, K. Maleski, B. Anasori, P. Lelyukh, L. Clark, Saleesha Sin and Y. Gogotsi, *Chem. Mater.*, 2017, **29**, 7633-7644.
3. X. Qian, X. Meng, J. Sun, L. Jiang, Y. Wang, J. Zhang, X. Hu, M. Shalom and J. Zhu, *ACS Appl. Mater. Interfaces* 2019, **11**, 27226-27232.
4. X. Fan, Y. Yang, X. Shi, Y. Liu, H. Li, J. Liang and Y. Chen, *Adv. Func. Mater.*, 2020, **2020**, 2007110.
5. M. Ju, Y. Yang, J. Zhao, X. Yin, Y. Wu and W. Que, *J. Adv. Dielectrics*, 2019, **9**, 1950047.
6. Y. Lu, D. Fan, H. Xu, H. Min, C. Lu, Z. Lin and X. Yang, *Solar RRL*, 2020, **4**, 2000232.
7. X. Ming, A. Guo, Q. Zhang, Z. Guo, F. Yu, B. Hou, Y. Wang, K. P. Homewood and X. Wang, *Carbon*, 2020, **167**, 285-295.
8. N. Ma, Q. Fu, Y. Hong, X. Hao, X. Wang, J. Ju and J. Sun, *ACS Appl. Mater. Interfaces* 2020, **12**, 18165-18173.
9. Z. Yu and P. Wu, *Adv. Mater. Tech.*, 2020, **5**, 2000065.
10. Q. Zhang, G. Yi, Z. Fu, H. Yu, S. Chen and X. Quan, *ACS Nano*, 2019, **13**, 13196-13207.
11. P. He, L. Hao, N. Liu, H. Bai, R. Niu and J. Gong, *Chem. Eng. J.*, 2021, **423** 130268.
12. T. Chen, Z. Wu, Z. Liu, J. T. Aladejana, X. Wang, M. Niu, Q. Wei and Y. Xie, *ACS Appl. Mater. Interfaces*, 2020, **12**, 19511-19518.
13. P. Liu, L. Miao, Z. Deng, J. Zhou, H. Su, L. Sun, S. Tanemura, W. Cao, F. Jiang and L. Zhao, *Mater. Today Energy*, 2018, **8**, 166-173.
14. D. Guo and X. Yang, *Sci. China Mater.*, 2019, **62**, 711-718.
15. C. Chen, Y. Li, J. Song, Z. Yang, Y. Kuang, E. Hitz, C. Jia, A. Gong, F. Jiang, J. Zhu, B. Yang, J. Xie and L. Hu, *Adv. Mater.*, 2017, **29**, 1701756.
16. H. Liu, C. Chen, G. Chen, Y. Kuang, X. Zhao, J. Song, C. Jia, X. Xu, E. Hitz, H. Xie, S. Wang, F. Jiang, T. Li, Y. J. Li, A. Gong, R. Yang, S. Das and L. B. Hu, *Adv. Energy Mater.*, 2018, **8**, 1701616.
17. H. C. Yang, Z. Chen, Y. Xie, J. Wang, J. W. Elam, W. Li and S. B. Darling, *Adv. Mater.*

Interfaces, 2019, **6**, 1801252.

18. W. Chao, X. Sun, Y. Li, G. Cao, R. Wang, C. Wang and S. H. Ho, *ACS Appl. Mater. Interfaces*, 2020, **12**, 22387-22397.
19. S. Chen, Z. Sun, W. Xiang, C. Shen, Z. Wang, X. Jia, J. Sun and C. J. Liu, *Nano Energy*, 2020, **76**, 104998.
20. Y. Zhang, S. K. Ravi, J. V. Vaghasiya and S. C. Tan, *iScience*, 2018, **3**, 31-39.
21. L. Yang, G. Chen, N. Zhang, Y. Xu and X. Xu, *ACS Sustainable Chem. Eng.*, 2019, **7**, 19311-19320.
22. N. Xu, X. Hu, W. Xu, X. Li, L. Zhou, S. Zhu and J. Zhu, *Adv. Mater.*, 2017, **29**, 1606762.
23. Y. Ito, Y. Tanabe, J. Han, T. Fujita, K. Tanigaki and M. Chen, *Adv. Mater.*, 2015, **27**, 4302-4307.
24. N. Liu, L. Hao, B. Zhang, R. Niu, J. Gong and T. Tang, *Sustainable Energy Fuels*, 2020, **4**, 5522-5532.
25. G. Wang, Y. Fu, X. Ma, W. Pi, D. Liu and X. Wang, *Carbon*, 2017, **114**, 117-124.
26. X. Hu, W. Xu, L. Zhou, Y. Tan, Y. Wang, S. Zhu and J. Zhu, *Adv. Mater.*, 2017, **29**, 1604031.
27. K. Kim, S. Yu, C. An, S. W. Kim and J. H. Jang, *ACS Appl. Mater. Interfaces*, 2018, **10**, 15602-15608.
28. X. Chen, C. Meng, Y. Wang, Q. Zhao, Y. Li, X. M. Chen, D. Yang, Y. Li and Y. Zhou, *ACS Sustainable Chem. Eng.*, 2020, **8**, 1095-1101.
29. L. Zhou, Y. Tan, D. Ji, B. Zhu, P. Zhang, J. Xu, Q. Gan, Z. Yu and J. Zhu, *Sci. Adv.*, 2016, **2**, e1501227.
30. L. Zhang, B. Tang, J. Wu, R. Li and P. Wang, *Adv. Mater.*, 2015, **27**, 4889-4894.
31. J. Jia, W. Liang, H. Sun, Z. Zhu, C. Wang and A. Li, *Chem. Eng. J.*, 2019, **361**, 999-1006.
32. L. Wang, C. Liu, H. Wang, Y. Xu, S. Ma, Y. Zhuang, W. Xu, W. Cui and H. Yang, *ACS Appl. Mater. Interfaces*, 2020, **12**, 24328-24338.